inorganics

MDPI

Article

Novel Fluoridoaluminates from Ammonothermal Synthesis: Two Modifications of K_2AlF_5 and the Elpasolite Rb_2KAlF_6

Christian Bäucker, Peter Becker, Keshia J. Morell and Rainer Niewa *

Institute of Inorganic Chemistry, University of Stuttgart, Pfaffenwaldring 55, 70569 Stuttgart, Germany; c.baeucker@gmail.com (C.B.); peter.heuberg@t-online.de (P.B.); keshia.morell@gmx.de (K.J.M.)
* Correspondence: rainer.niewa@iac.uni-stuttgart.de

Abstract: Two new modifications of the pentafluoridoaluminate K_2AlF_5 were obtained from ammonothermal synthesis at 753 K, 224 MPa and 773 K, 220 MPa, respectively. Both crystallize in the orthorhombic space group type *Pbcn*, with close metric relations and feature kinked chains of *cis*-vertex-connected AlF_6 octahedra resulting in the Niggli formula $^1_\infty\{[AlF_{2/2}{}^eF_{4/1}{}^t]^{2-}\}$. The differences lie in the number of octahedra necessary for repetition within the chains, which for K_2AlF_5-2 is realized after four and for K_2AlF_5-3 after eight octahedra. As a result, the orthorhombic unit cell for K_2AlF_5-3 is doubled in chain prolongation direction [001] as compared to K_2AlF_5-2 (1971.18(4) pm versus 988.45(3) pm, respectively), while the unit cell parameters within the other two directions are virtually identical. Moreover, the new elpasolite Rb_2KAlF_6 is reported, crystallizing in the cubic space group $Fm\bar{3}m$ with a = 868.9(1) pm and obtained under ammonothermal conditions at 723 K and 152 MPa.

Keywords: ammonothermal synthesis; fluoride; aluminum

Citation: Bäucker, C.; Becker, P.; Morell, K.J.; Niewa, R. Novel Fluoridoaluminates from Ammonothermal Synthesis: Two Modifications of K_2AlF_5 and the Elpasolite Rb_2KAlF_6. *Inorganics* **2022**, *10*, 7. https://doi.org/10.3390/inorganics10010007

Academic Editor: Hans-Conrad zur Loye

Received: 19 December 2021
Accepted: 8 January 2022
Published: 10 January 2022

1. Introduction

Ammonothermal synthesis, which uses supercritical ammonia as a solvent medium, is a pathway to the production and crystal growth of a variety of materials, particularly nitrides, amides, and even halides, depending on the administered mineralizer [1,2]. Especially due to the available nitrides from ammonothermal reactions, such as AlN [3], GaN [4,5], and InN [6], this technique has gained considerable interest [7]. Exploratory work in ammonothermal synthesis recently led to solid intermediate amides, which may give valuable information about the dissolved species during the process as well as the condensation process eventually producing nitride materials [8–10]. Similar to the hydrothermal technique, we frequently observe the formation of several modifications of the same compound under rather similar pressure–temperature conditions during synthesis [11].

For ammonothermal synthesis, typically supercritical conditions are applied (critical point of pure ammonia at 405.2 K and 11.3 MPa [12]), which are most often realized by applying elevated temperatures to a sealed reaction vessel, therefore reaching a high pressure from the expanding ammonia contained within. In this experimental set-up, pressure and thus ammonia density fundamentally depend on the temperature and filling degree of the autoclave with ammonia. The supercritical state of the solvent in combination with suitable mineralizers is intended to provide sufficient solubility and supersaturation for solid product formation and ideally crystal growth. The mineralizer can provide ammonobasic or ammonoacidic conditions within a wide range of pH and serves for the formation of dissolved complex species.

K_2AlF_5 was first reported by de Kozak et al. as a dehydrate of $K_2AlF_5{\cdot}H_2O$, which was obtained by hydrothermal synthesis [13]. During thermogravimetric investigations, the water-free K_2AlF_5 was observed to form upon heating. In the crystal structure of the

monohydrate, very slightly kinked infinite trans-vertex-sharing octahedra with Niggli formula $^{1}_{\infty}\{[AlF_{2/2}{}^{e}F_{4/1}{}^{t}]^{2-}\}$ (e = corner-sharing, t = terminal) are prearranged to result in straight chains in the dehydrate. This compound, in the following denoted K_2AlF_5-1, crystallizes in *P*4/*mmm* and spontaneously transforms back to its monohydrate after days in air. While these fluoridoaluminates are characterized by infinite chains of trans-vertex-sharing octahedra around Al, isolated octahedra $[AlF_6]^{3-}$ are well known, for example from the mineral elpasolite, K_2NaAlF_6 [14,15], which might be described as a double perovskite. Fluorides with the elpasolite structure are numerous [14,16,17]. Here we report two new modifications of K_2AlF_5 featuring infinite chains of cis-vertex-sharing octahedra around Al with different conformations and the novel elpasolite Rb_2KAlF_6, obtained from ammonothermal synthesis using a mineralizer system containing alkali metal amides and fluoride ions in a near-ammononeutral regime.

2. Results

Two new modifications of K_2AlF_5 were obtained from supercritical ammonia under very similar conditions of 753 K, 224 MPa versus 773 K, 220 MPa. While we monitor the pressure in the autoclaves during the process, the temperatures given represent the furnace temperatures outside the autoclave. Average temperatures within the autoclave are about 100 K lower, and an intended temperature gradient of about 50 K naturally develops due to heat loss at the autoclave installations for filling, pressure monitoring, and safety purposes sticking out the furnace [18]. Thus from experimental conditions, we cannot derive any information on the relative stabilities of these different modifications. Upon providing both potassium and rubidium ions in solution at slightly reduced pressures (723 K and 152 MPa) the novel elpasolite Rb_2KAlF_6 was formed.

All three fluoridoaluminates were obtained as colorless crystals in the hot zone of the autoclave in a temperature gradient, thus exhibiting lower solubility at higher temperatures for the given conditions (so-called retrograde solubility). The temperature dependence of the solubility for a given mineralizer system typically depends on the pressure and temperature regime applied [2,19]. The mineralizer system itself has a fundamental impact on solubility and temperature dependence via the formation of dissolved species and intermediates. Here we used a combination of metal fluorides and alkali metal amides in molar ratios such that near-ammononeutral conditions are expected if completely reacted. While the dissolved intermediates are difficult to experimentally study in situ due to the extreme conditions administered, it is likely that they are represented in the present case by complex fluoridoaluminate ions.

2.1. Crystal Structures

Potassium Pentafluoridoaluminates K_2AlF_5

We present two novel modifications of K_2AlF_5, which both crystallize in the orthorhombic space group type *Pbcn* and are labeled K_2AlF_5-2 and K_2AlF_5-3 in the following. According to structure determination from single-crystal X-ray diffraction, K_2AlF_5-3 (Figure 1, bottom) features a doubled *c*-axis in comparison to K_2AlF_5-2 (Figure 1, top), while the *a* and *b* axes are nearly identical. This fact can readily be understood from the crystal structures discussed in the following. Selected crystallographic data and refinement parameters are gathered in Table 1. Fractional atomic coordinates and isotropic displacement parameters of K_2AlF_5-2 and K_2AlF_5-3 can be found in Tables 2 and 3, respectively.

The crystal structure of K_2AlF_5-2 (Figure 1, top) features *cis*-vertex-sharing AlF_6-octahedra, which form infinite zig-zag chains running parallel [001]. These chains obey the Niggli formula $^{1}_{\infty}\{[AlF_{2/2}{}^{e}F_{4/1}{}^{t}]^{2-}\}$ and are aligned in the motif of a hexagonal rod packing (Figure 2, left). Repetition of the zig-zag chain is realized after four octahedra. The terminal fluoride ligands F(1–4) feature Al–F distances in the range of 176 pm to 179 pm, which is noticeably shorter than the distances to the bridging fluorides atoms (F(5) with 189 pm and F(6) with 192 pm). Selected interatomic distances are gathered in Table 4. Despite these slightly different distances, the octahedra are close to ideal as indicated by the

internal angles near 90° and 180°. The angles at the bridging fluoride ligands ∢ (Al–F–Al) vary from linear (180° due to symmetry restrictions) to slightly kinked with 168° at F(5) and F(6), respectively.

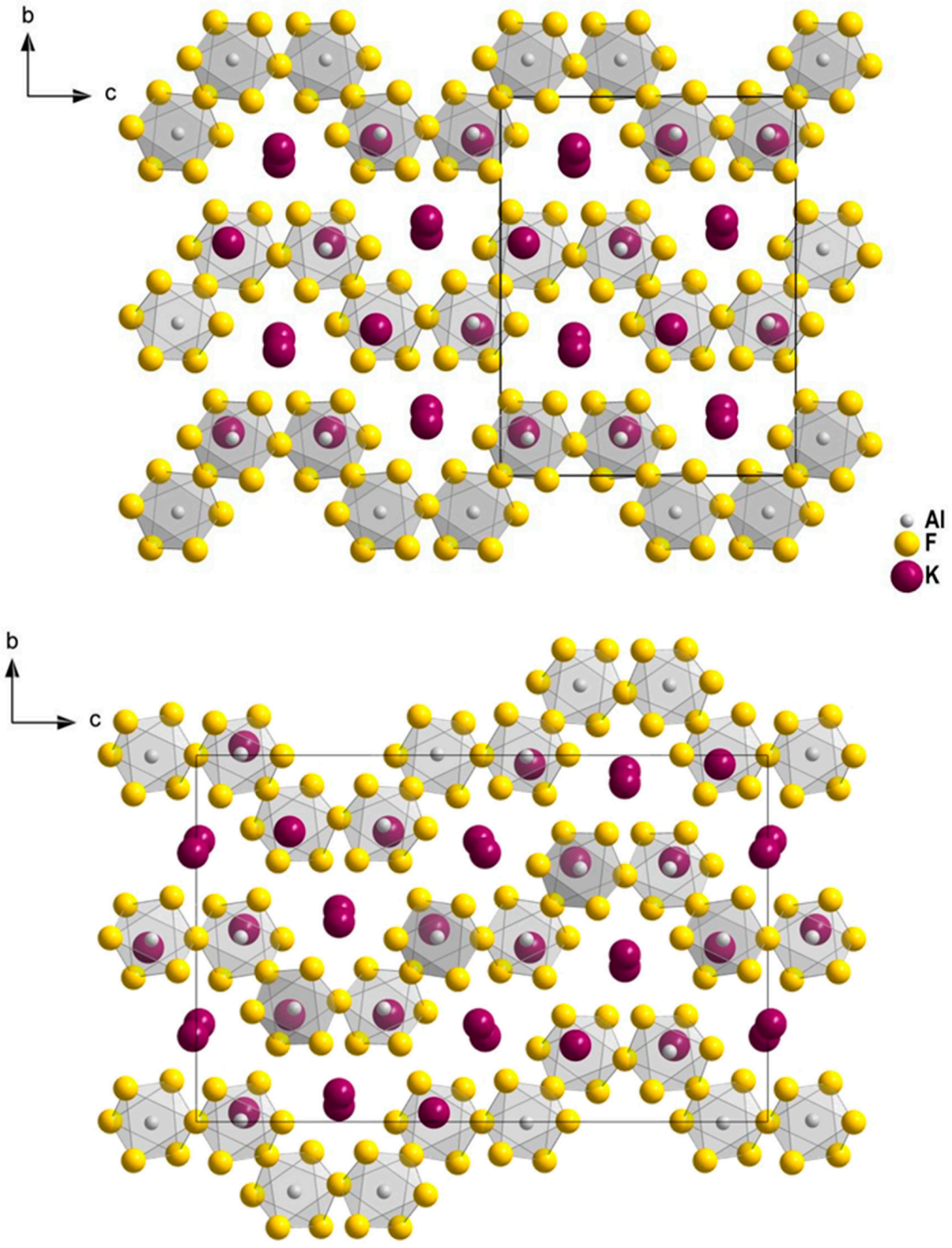

Figure 1. Sections of the crystal structures of K_2AlF_5-2 (**top**) and K_2AlF_5-3 (**bottom**), viewing direction [100].

Table 1. Selected crystallographic parameters and refinement data of K_2AlF_5-2, K_2AlF_5-3, and Rb_2KAlF_6.

Compound	**K_2AlF_5-2**	**K_2AlF_5-3**	**Rb_2KAlF_6**
Crystal system	Orthorhombic	Orthorhombic	Cubic
Space group	*Pbcn*	*Pbcn*	Fm $\bar{3}m$
a/pm	718.12(3)	718.370(10)	868.88(11)
b/pm	1265.94(5)	1264.49(2)	-
c/pm	988.45(3)	1971.18(4)	-
Z	8	16	4
Density (calculated)/g·cm^{-3}	2.959	2.970	3.554
Volume/10^6 pm^3	898.60(6)	1790.56(5)	656.0(2)
Index ranges *hkl*	$-9 \le h \le 9$ $-16 \le k \le 16$ $-12 \le l \le 11$	$-9 \le h \le 8$ $-16 \le k \le 16$ $-25 \le l \le 25$	$-10 \le h \le 9$ $-10 \le k \le 10$ $-11 \le l \le 11$
$2\theta_{max}/^\circ$	54.94	54.96	54.96
F(000)	768	1536	640
T/K	293(2)	293(2)	293(2)
μ(Mo-K$_\alpha$)/mm^{-1}	2.30	2.31	15.73
Measured reflections/sym. independent	14490/1034	27919/2061	1072/58
R_{int}/R_σ	0.0857/0.0357	0.0557/0.0201	0.1148/0.0319
R_1 with $\|F_o\| > 4\sigma(F_o)$	0.0308	0.0219	0.0318
$R_1/wR_2/GooF$	0.0517/0.0732/1.107	0.0287/0.0554/1.112	0.0392/0.0949/1.189
Largest peak/hole in the difference electron density map/10^6 pm^{-3}	0.64/–0.43	0.31/–0.32	0.85/–0.41

Table 2. Fractional atomic coordinates and equivalent isotropic displacement parameters (in 10^4 pm^2) for K_2AlF_5-2.

Atom	**Site**	***x*/*a***	***y*/*b***	***z*/*c***	U_{eq}
Al	8*d*	0.1544(1)	0.09746(6)	0.40752(7)	0.0148(2)
F(1)	8*d*	0.0028(2)	0.1963(1)	0.4657(2)	0.0237(4)
F(2)	8*d*	0.2039(2)	0.3988(1)	0.0533(2)	0.0248(4)
F(3)	8*d*	0.2149(2)	0.4889(1)	0.3435(2)	0.0242(4)
F(4)	8*d*	0.2904(2)	0.1911(1)	0.3155(2)	0.0234(4)
F(5)	4*a*	0	0	0	0.0224(5)
F(6)	4*c*	0	0.0811(2)	1/4	0.0215(5)
K(1)	4*c*	0	0.32802(6)	1/4	0.0216(2)
K(2)	8*d*	0.35685(9)	0.11414(5)	0.07843(6)	0.0288(2)
K(3)	4*c*	1/2	0.36182(6)	1/4	0.0238(2)

Table 3. Fractional atomic coordinates and equivalent isotropic displacement parameters (in 10^4 pm^2) for K_2AlF_5-3.

Atom	**Site**	***x*/*a***	***y*/*b***	***z*/*c***	U_{eq}
Al(1)	8*d*	0.34006(6)	0.00306(4)	0.07804(2)	0.01285(12)
Al(2)	8*d*	0.15454(6)	0.30892(4)	0.32833(2)	0.01289(12)
F(1)	8*d*	0.00118(13)	0.21130(8)	0.14313(5)	0.02101(22)
F(2)	8*d*	0.00529(13)	0.40872(8)	0.37647(5)	0.02002(22)
F(3)	4*b*	0	1/2	0	0.01986(30)
F(4)	4*c*	0	0.32874(11)	1/4	0.01899(29)
F(5)	8*d*	0.28728(14)	0.21407(8)	0.28163(5)	0.02057(22)

Table 3. *Cont.*

Atom	Site	*x*/*a*	*y*/*b*	*z*/*c*	U_{eq}
F(6)	8*d*	0.27138(14)	0.38826(7)	0.04254(5)	0.01934(21)
F(7)	8*d*	0.47905(14)	0.10612(8)	0.10966(5)	0.02259(23)
F(8)	8*d*	0.30459(14)	0.49862(8)	0.15048(5)	0.02174(23)
F(9)	8*d*	0.19137(14)	0.08868(8)	0.03231(5)	0.02165(23)
F(10)	8*d*	0.28759(14)	0.41739(8)	0.29745(5)	0.02110(22)
F(11)	8*d*	0.29631(14)	0.30022(8)	0.40163(5)	0.02154(22)
K(1)	4*c*	1/2	0.04458(4)	1/4	0.02156(13)
K(2)	4*c*	0	0.07646(4)	1/4	0.01799(13)
K(3)	8*d*	0.15370(5)	0.02462(3)	0.41609(2)	0.02395(11)
K(4)	8*d*	0.36071(5)	0.29171(3)	0.16355(2)	0.02299(11)
K(5)	8*d*	0.01092(5)	0.26658(3)	0.49444(2)	0.01940(11)

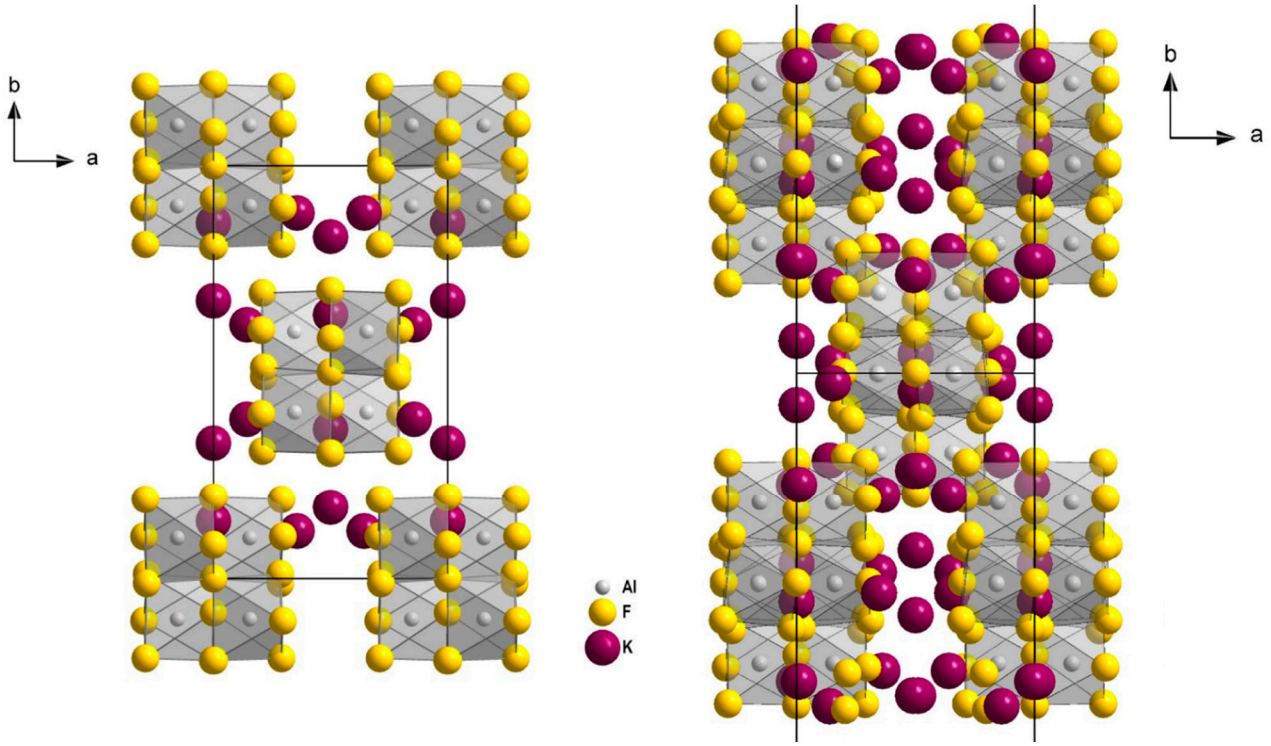

Figure 2. Section of the crystal structures of K_2AlF_5-2 (**left**) and K_2AlF_5-3 (**right**), shown along [001] emphasizing the motif of hexagonal rod packings by the infinite fluoroaluminate chains. The crystallographic unit cells are indicated by black lines.

Table 4. Selected interatomic distances (in pm) in K_2AlF_5-2.

	Distance/pm		Distance/pm		Distance/pm		Distance/pm
Al–F(1)	175.5(2)	K(1)–F(2)	259.4(2)	K(2)–F(4)	258.3(2)	K(3)–F(4)	271.2(2)
Al–F(2)	176.5(2)	K(1)–F(2)	259.4(2)	K(2)–F(3)	271.3(2)	K(3)–F(4)	271.2(2)
Al–F(3)	178.1(2)	K(1)–F(1)	270.6(2)	K(2)–F(2)	277.2(2)	K(3)–F(3)	276.3(2)
Al–F(4)	178.5(2)	K(1)–F(1)	270.7(2)	K(2)–F(2)	281.7(2)	K(3)–F(3)	276.3(2)
Al–F(5)	189.37(7)	K(1)–F(3)	271.7(2)	K(2)–F(1)	281.8(2)	K(1)–F(6)	277.6(2)
Al–F(6)	192.24(8)	K(1)–F(3)	271.7(2)	K(2)–F(1)	283.1(2)	K(3)–F(1)	290.5(2)
		K(1)–F(4)	278.8(2)	K(2)–F(4)	291.0(2)	K(3)–F(1)	290.5(2)
		K(1)–F(4)	278.8(2)	K(2)–F(5)	304.23(7)	K(3)–F(2)	291.9(2)
		K(1)–F(6)	312.6(2)	K(2)–F(6)	310.13(7)	K(3)–F(2)	291.9(2)
				K(2)–F(3)	310.6(2)	K(3)–F(5)	302.76(5)
				K(2)–F(3)	311.8(2)	K(3)–F(5)	302.76(5)

The potassium ions interconnect three chains each (Figure 3). As it can be taken from Figure 4, K(1) is coordinated by nine fluoride ions, K(2) and K(3) by eleven fluoride ligands. Coordination by the octahedra of the chains is realized mono-, bi-, and tridentate. Distances with about 258 to 312 pm are in the expected range, given those found for K_2AlF_5-1, K_2AlF_5-3, and Rb_2KAlF_6 discussed below.

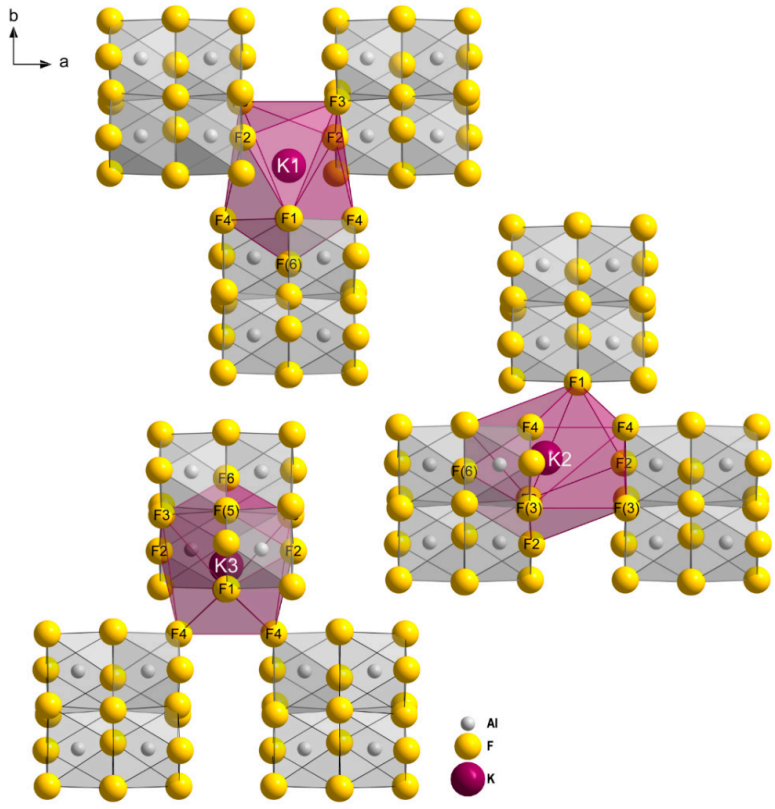

Figure 3. Interconnection of the infinite fluoridoaluminate zig-zag chains by potassium ions in K_2AlF_5-2.

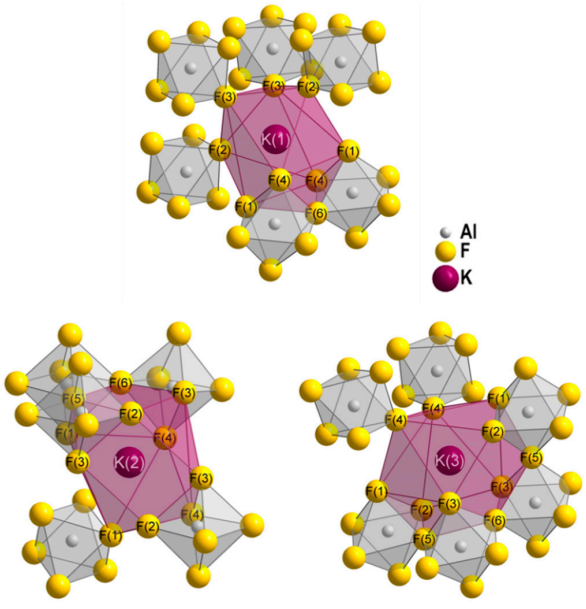

Figure 4. Potassium site coordination by AlF_6-octahedra in K_2AlF_5-2. Each potassium site connects three fluoridoaluminate chains.

Similar to K_2AlF_5-2, K_2AlF_5-3 crystallizes in the orthorhombic space group type *Pbcn*, but with a doubled *c*-axis (Figure 1, bottom). It crystallizes as an isotype of K_2FeF_5, first described by Vlasse et al. in the noncentrosymmetric space group type $Pn2_1a$, which was later corrected by Le Bail et al. [20,21]. The crystal structure of K_2AlF_5-3 shows close structural similarity to K_2AlF_5-2, while apparently no direct group–subgroup relation exists. The crystal structure of K_2AlF_5-3 also contains infinite zig-zag chains of *cis*-vertex-sharing AlF_6-octahedra, which are aligned parallel [001] in the motif of a hexagonal rod packing (Figure 2, right) and consistent with the Niggli formula $^{1}_{\infty}\{[AlF_{2/2}{}^{e}F_{4/1}{}^{t}]^{2-}\}$. However, in K_2AlF_5-3 the chains exhibit a longer repetition length, completed only after eight octahedra. Figure 1 gives a comparison of the arrangements of the chains in K_2AlF_5-2 and K_2AlF_5-3. The already known modification K_2AlF_5-1 (Cs_2MnF_5 structure type in $P4/mmm$ with $a \approx 597$ pm, $c \approx 370$ pm), in contrast, is built from straight chains of *trans*-vertex-sharing octahedra with a 180° angle at the bridging fluoride ligands (Figure 5) [13]. The coordination polyhedron of potassium can be described as a bicapped square prism.

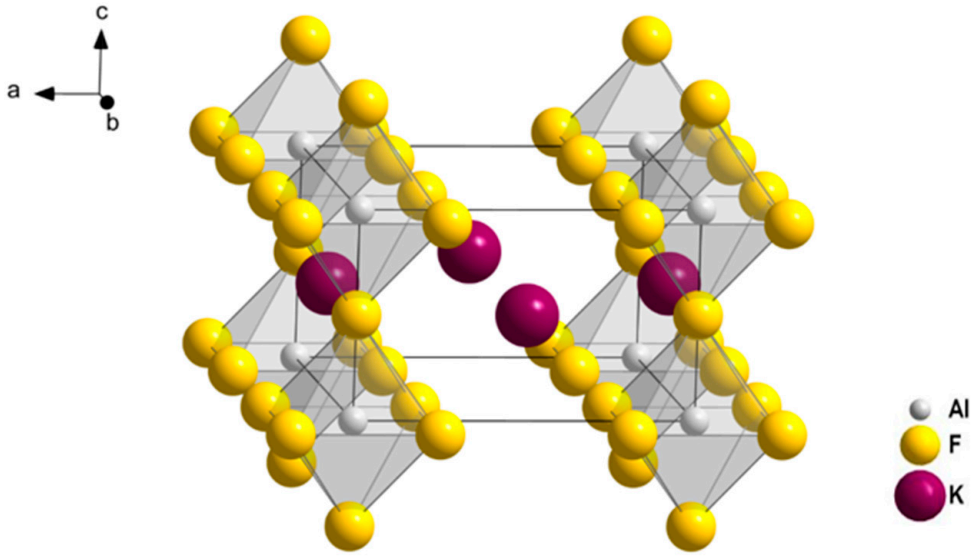

Figure 5. Section of the crystal structure of K_2AlF_5-1 according to [13].

The five different potassium sites in K_2AlF_5-3 are coordinated by nine, ten, or eleven fluoride ions (see Figure 6). In contrast to K_2AlF_5-2, the coordination by the octahedra of the chains is only realized mono- or three-dentate, but no bi-dentate coordination appears. Each site connects three chains of AlF_6-octahedra, similar to the situation in K_2AlF_5-2 (see Figure 7). Still, internal distances in both modifications are rather similar: *d*(Al–F) in K_2AlF_5-3 to terminal fluoride ligands range from 176 pm to 180 pm, while those to bridging fluoride ions are longer with 191 and 192 pm (Table 5). Again the internal angles within the octahedra are close to ideal the of 90° and 180°, while the angles at the bridging fluoride ions ∢ (Al–F–Al) diversify between 180° for F(3) (due to symmetry restrictions) and 165° at F(4). Distances between potassium and fluoride ions in both modifications are also rather similar, although the furthest distances in the coordination are increased to 334 pm in K_2AlF_5-3.

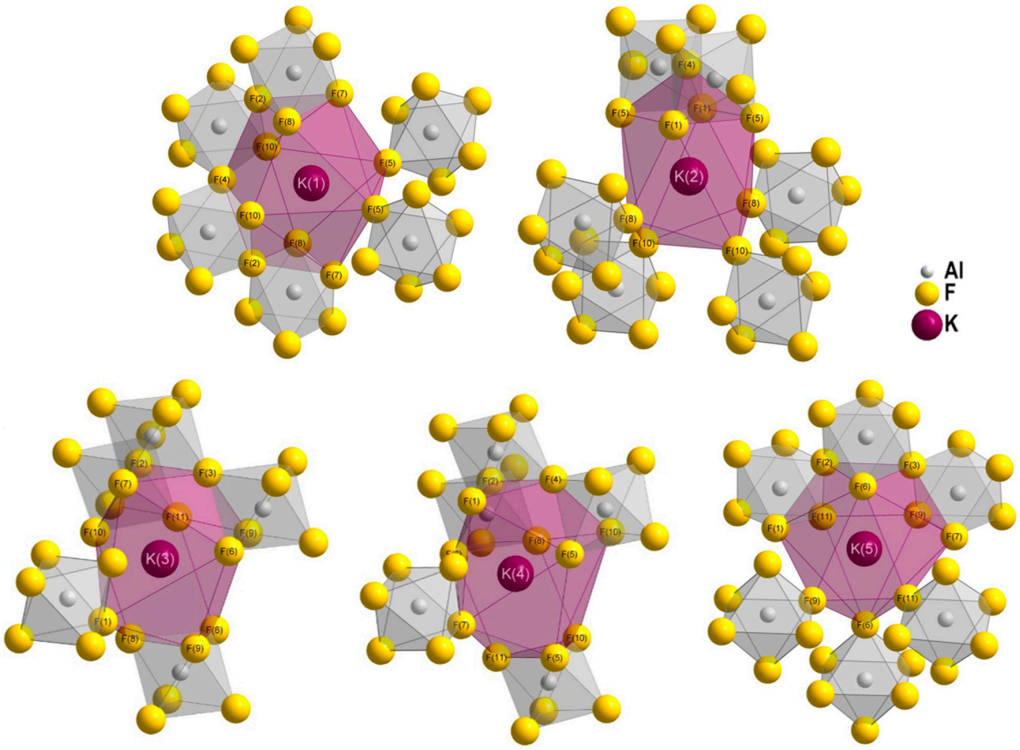

Figure 6. Potassium site coordination by AlF_6-octahedra in K_2AlF_5-3. Each site connects three fluoridoaluminate chains.

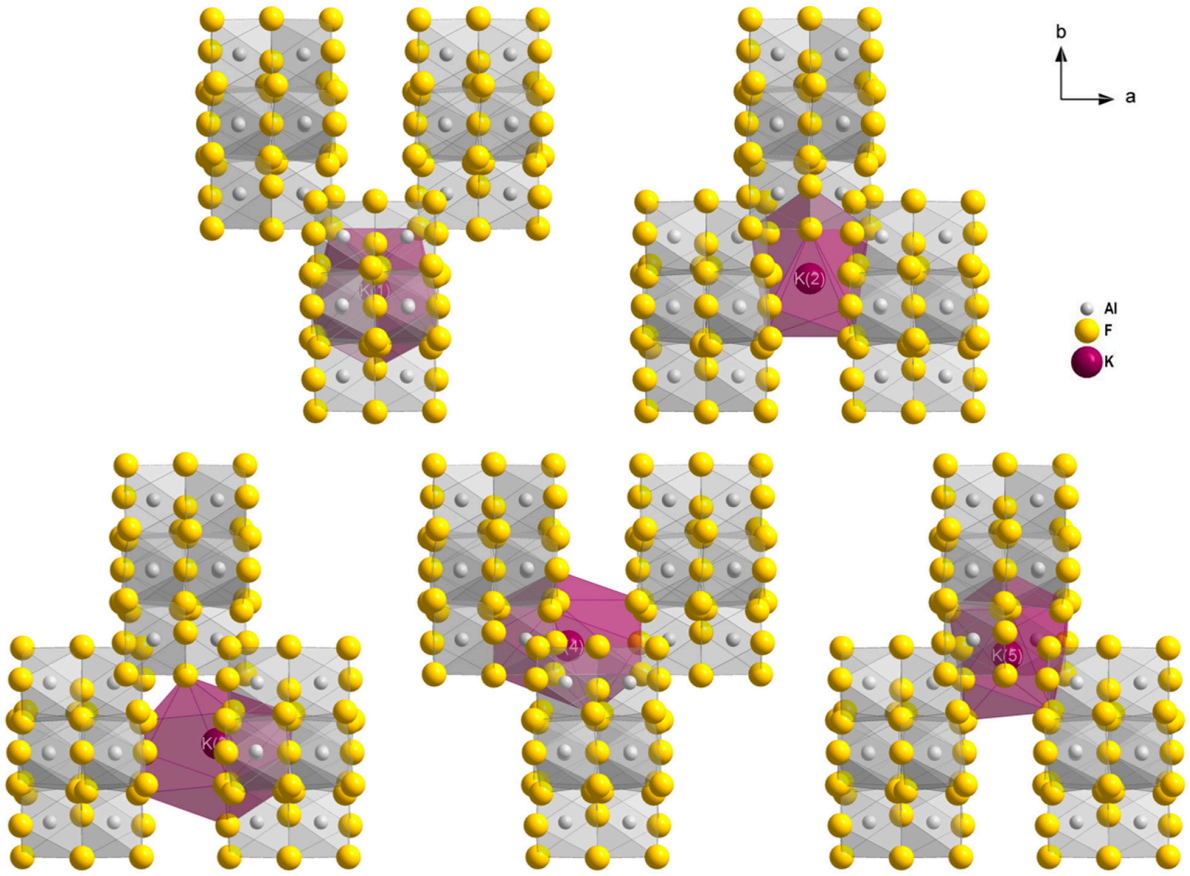

Figure 7. Interconnection of the infinite fluoridoaluminate zig-zag chains by potassium ions in K_2AlF_5-3.

Table 5. Selected interatomic distances (in pm) in K_2AlF_5-3.

	Distance/pm		Distance/pm		Distance/pm		Distance/pm
Al(1)–F(7)	175.60(11)	Al(2)–F(1)	175.82(10)	K(1)–F(5)	2 × 270.50(10)	K(2)–F(8)	2 × 260.54(9)
Al(1)–F(8)	176.68(10)	Al(2)–F(11)	177.12(10)	K(1)–F(4)	1 × 272.93(15)	K(2)–F(10)	2 × 269.24(10)
Al(1)–F(9)	176.79(10)	Al(2)–F(10)	177.92(10)	K(1)–F(10)	2 × 278.02(11)	K(2)–F(1)	2 × 271.02(10)
Al(1)–F(6)	179.95(10)	Al(2)–F(5)	178.75(10)	K(1)–F(7)	2 × 287.76(10)	K(2)–F(5)	2 × 277.05(11)
Al(1)–F(2)	190.68(10)	Al(2)–F(2)	190.85(10)	K(1)–F(8)	2 × 299.57(10)	K(2)–F(4)	1 × 319.00(15)
Al(1)–F(3)	192.04(5)	Al(2)–F(4)	191.82(5)	K(1)–F(2)	2 × 302.77(10)		
K(3)–F(9)	271.56(10)	K(4)–F(5)	258.05(10)	K(5)–F(6)	264.78(11)		
K(3)–F(10)	273.60(10)	K(4)–F(8)	265.97(10)	K(5)–F(6)	267.91(10)		
K(3)–F(6)	277.78(10)	K(4)–F(7)	271.27(11)	K(5)–F(11)	269.94(10)		
K(3)–F(9)	279.92(11)	K(4)–F(6)	275.55(10)	K(5)–F(9)	272.95(10)		
K(3)–F(8)	284.93(11)	K(4)–F(11)	278.09(11)	K(5)–F(11)	278.04(11)		
K(3)–F(1)	285.88(11)	K(4)–F(1)	280.47(11)	K(5)–F(7)	278.49(11)		
K(3)–F(11)	287.44(11)	K(4)–F(5)	291.99(11)	K(5)–F(1)	280.16(10)		
K(3)–F(7)	287.75(11)	K(4)–F(10)	308.22(11)	K(5)–F(9)	291.23(11)		
K(3)–F(2)	295.96(10)	K(4)–F(2)	311.84(10)	K(5)–F(2)	293.93(10)		
K(3)–F(3)	300.36(4)	K(4)–F(10)	312.53(11)	K(5)–F(3)	295.47(4)		
K(3)–F(6)	334.39(11)	K(4)–F(4)	313.65(4)				

2.2. Raman Spectroscopy

The Raman signals obtained from single crystals of K_2AlF_5-2 and K_2AlF_5-3 are assigned in accordance with spectra reported for K_3AlF_6 [22], Na_3AlF_6 [23], and KF:AlF_3 melts [24]. The Raman spectra resulted in three signals between 700 and 300 cm^{-1} for both K_2AlF_5-2 and K_2AlF_5-3 (Figure 8). The two strong and sharp signals at approximately 600 and 456 cm^{-1} can be assigned to the Al–F stretching modes ν_1 and ν_2. The third signal at around 377 cm^{-1} is rather weak and belongs to the F–Al–F bending mode. The remaining signals below 300 cm^{-1} relate to lattice vibration modes with signals at 282, 190, 160, and 71 cm^{-1} for K_2AlF_5-2 and 240, 178, and 65 cm^{-1} for K_2AlF_5-3, respectively.

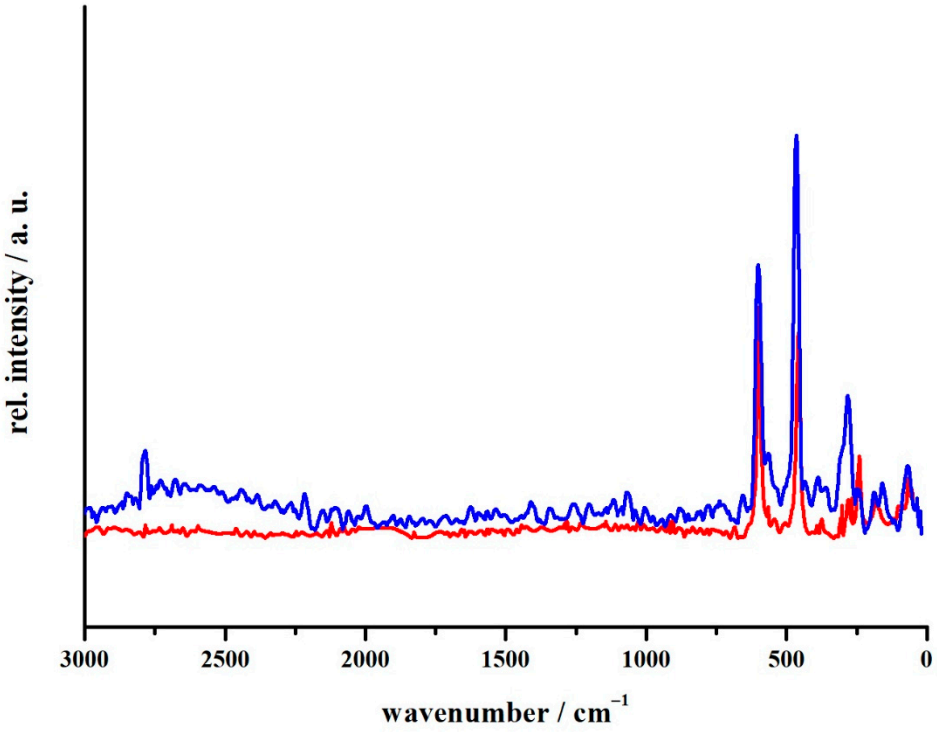

Figure 8. Raman spectra of K_2AlF_5-2 (blue) and K_2AlF_5-3 (red).

Compared with the literature, the observed signals are shifted to higher wavenumbers. However, literature data are from compounds containing isolated complex $[AlF_6]^{3-}$ ions and are mostly concerned with salt melts at higher temperatures, for which a shift of signals towards lower wavenumbers with rising temperature is reported [25].

Potassium Dirubidium Hexafluoridoaluminate, Rb_2KAlF_6

In an experiment, providing rubidium next to potassium ions within the reaction vessel, a new cubic hexafluoridoaluminate with elpasolite structure, Rb_2KAlF_6, was obtained. General crystallographic parameters are gathered in Table 1, the fractional atomic coordinates, as well as isotropic displacement parameters, are collected in Table 6. The structure features one crystallographic site each for aluminum, fluoride, potassium, and rubidium arranged in an ordered double perovskite motif with an alternating filling of octahedra formed from fluoride ions by aluminum and potassium ions. Consequently, the structure contains mutually isolated $[AlF_6]^{3-}$ octahedra arranged in the motif of a cubic closed packing. In this hierarchical view, potassium ions occupy octahedral voids, while rubidium ions are located in tetrahedral voids in the packing of $[AlF_6]^{3-}$ octahedra. This leads to twelvefold coordination of Rb by F in a distorted cuboctahedron (4 × triangular face of $[AlF_6]^{3-}$ octahedra, Figure 9). A slight antisite disorder by mutual substitution of potassium and rubidium ions appears possible, while refinements resulted in around 5% for both alkali metal sites. However, since for both sites the resulting figures are in the order of the standard deviations and the number of 58 unique reflections is already low in comparison to the number of refined parameters (7 for the fully ordered structure) we have discarded to further consider this minor disorder. Isostructural fluoridoaluminates comprise K_2LiAlF_6 [16], K_2NaAlF_6 [14], and Rb_2NaAlF_6 [17].

Table 6. Fractional atomic coordinates and equivalent isotropic displacement parameters (in 10^4 pm^2) of Rb_2KAlF_6.

Atom	Site	*x*/*a*	*y*/*b*	*z*/*c*	U_{eq}
Al	4*a*	0	0	0	0.0166(17)
K	4*b*	1/2	0	0	0.0224(14)
Rb	8*c*	1/4	1/4	1/4	0.0310(8)
F	24*e*	0	0.2073(8)	0	0.0386(18)

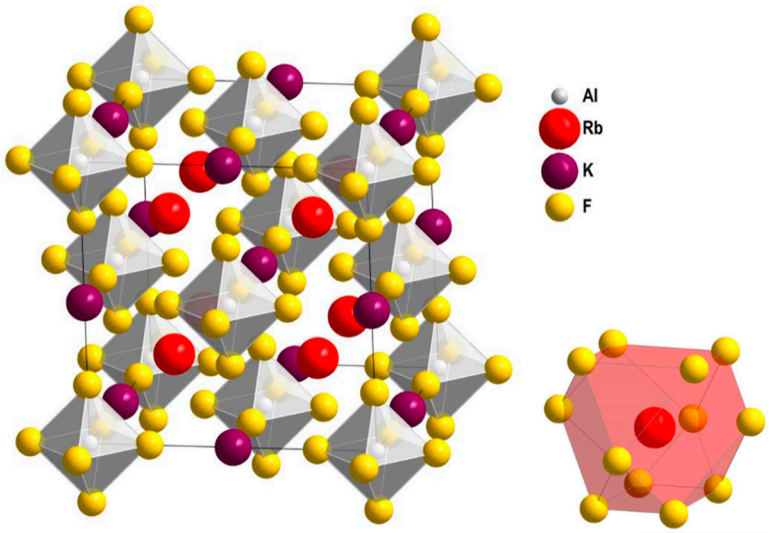

Figure 9. Extended unit cell of Rb_2KAlF_6 (**left**) and distorted cuboctahedral coordination of rubidium ions (**right**).

Distances within Rb_2KAlF_6 are within the expected ranges, with d(Al–F) = 180.1(7) pm, d(K–F) = 254.3(7) pm, and d(Rb–F) = 309.4(1) pm. Compared to the above-discussed

modifications of K_2AlF_5, the slightly longer distance of the terminal fluoride ligands to aluminum reflects the isolated complex ions $[AlF_6]^{3-}$ including the increased negative charge. The distance between potassium and fluoride ions, on the other hand, presents as shorter, due to the reduced coordination number of six.

3. Materials and Methods

The entire handling of all compounds was conducted under argon with $p(O_2) < 0.1$ ppm (glovebox: MBRAUN Inertgas-Systeme, Garching, Germany). The synthesis of the reported compounds was performed under similar conditions as discussed for the synthesis of intermediates in ammonothermal InN synthesis [6,26]. A custom-made autoclave from nickel base alloy was used, as well as a Si_3N_4 liner (air-pressure sintered silicon nitride, Ingenieurkeramik, a QSIL company, Frankenblick, Germany), which protects the autoclave from corrosion [27,28]. The autoclaves were assembled and disassembled in the glovebox. Ammonia (Linde, Pullach, Germany, purity $\geq$ 99.999) was filled into the autoclave by condensation (cooling in an ethanol/dry ice bath), using a self-made tensi-eudiometer according to Hüttig [29]. The synthesis was performed in a one-zone tubular furnace (LOBA 1200-60-400-1 OW, HTM Reetz, Berlin, Germany) set up in a vertical position, generating a temperature gradient from the heated lower part of the reaction vessel (warmer temperature zone) to the unheated upper part (colder temperature zone) [30,31]. The pressure was monitored with a pressure transmitter and a digital analyzer (HBM P2VA2 and DA 2510, Hottinger Brüel and Kjaer, Darmstadt, Germany).

For the synthesis of K_2AlF_5-2, equimolar amounts of InF_3 (125.4 mg, 0.73 mmol) and AlF_3 (61.3 mg, 0.73 mmol) were used as aluminum and fluoride sources together with a sixfold amount of KNH_2 (241.3 mg, 4.38 mmol), which served as mineralizer and provided the potassium (equimolar amounts of F^- and K^+). At the beginning of the experiment, KNH_2 was spatially separated from the metal fluorides by placing in a Si_3N_4 crucible, equipped with a cap with a hole. The crucible prevents the reactants and mineralizer from a premature solid-state reaction, the cap reduces the diffusion rate of dissolved KNH_2 into the solution. A total of 19.0 g ammonia were condensed into the autoclave, which corresponds to a filling degree of 100% regarding the free volume in the liner and crucible. The autoclave was heated up to 753 K within five hours and maintained at this temperature for 60 h, reaching a maximum pressure of 224 MPa. It was subsequently cooled within 15 h to room temperature. K_2AlF_5-3 was obtained from a synthesis using Al (50.0 mg, 1.85 mmol), Cr (96.4 mg, 1.85 mmol), NH_4F (205.7, 5.56 mmol), and KNH_2 (306.4 mg, 5.56 mmol) in 17.0 g of ammonia (90% filling degree), again providing equimolar amounts of the ammonoacid and the ammonobase. The autoclave was heated to 773 K within five hours and kept at that temperature for 24 h. At maximum, a pressure of 220 bar was reached. The autoclave was subsequently cooled to room temperature over a time of 48 h. Both products were obtained as colorless crystals from the hot zone of the autoclave. Chromium and indium were not found to take part in the reactions.

The synthesis of Rb_2KAlF_6 included AlF_3 (90.7 mg, 1.08 mmol), Ga (75.3 mg, 1.08 mmol), NH_4F (119.5 mg, 3.23 mmol), and $RbNH_2$ (355.4 mg, 6.45 mmol), residue KNH_2 from earlier reactions, and a total of 17.5 g ammonia (93% filling degree). Loaded with the starting chemicals, the autoclave was heated to 723 K within 4.5 h and then kept at that temperature for 72 h, reaching a maximum pressure of 152 MPa. Subsequently, the autoclave was cooled to room temperature within 72 h, after which the product was found in the hot zone of the autoclave. Elemental gallium was recovered unchanged after the reaction.

InF_3 (Alfa Aesar, Thermo Fisher, Kandel, Germany, 99.95% metal basis, anhydrous), AlF_3 (abcr, Karlsruhe, Germany, 99.99% metal basis), Al (Alfa Aesar, Thermo Fischer Kandel GmbH, Germany, 99.97% metal basis), Cr (Sigma Aldrich, Taufkirchen, Germany, 99.0%), NH_4F (Sigma Aldrich, Taufkirchen, Germany, 99.99%), and self-made KNH_2 and $RbNH_2$, synthesized from potassium (Sigma Aldrich, Merck, Darmstadt, Germany, 98%) and rubidium (donation) reacting with ammonia at 373 K for 24 h were used for synthesis.

Single-crystal X-ray diffraction data collection was performed on a κ-CCD (Bruker Cooperation, Billerica, MA, USA) with Mo-K_α radiation. Solving and refinement of all crystal structures was done with the SHELX-2013 software package [32,33].

Single-crystal Raman spectroscopy was done on an XploRa Raman spectrometer (Horiba Europe, Oberursel, Germany) equipped with a confocal polarization microscope (Olympus BX51, Olympus Europa, Hamburg, Germany). For single-crystal X-ray diffraction and Raman spectroscopy, the crystals were measured in a sealed glass capillary.

4. Conclusions

Ammonothermal synthesis in presence of fluoride ions is a promising technique for the production of complex fluorides including new modifications, which possibly are difficult to assess by other methods. We have obtained two new modifications of K_2AlF_5, build up by zig-zag chains of *cis*-vertex-sharing AlF_6-octahedra with different conformations. Upon addition of rubidium next to potassium ions within the system, formation of the quaternary elpasolite, Rb_2KAlF_6, is preferred, which contains mutually isolated $[AlF_6]^{3-}$ octahedra.

Author Contributions: Conceptualization, C.B., P.B. and R.N.; methodology, C.B., P.B. and K.J.M.; formal analysis, C.B., P.B. and K.J.M.; investigation, C.B., P.B. and K.J.M.; resources, R.N.; data curation, C.B., P.B. and K.J.M.; writing—original draft preparation, C.B., P.B. and R.N.; writing—review and editing, C.B., P.B. and R.N.; visualization, C.B. and P.B.; supervision, R.N.; project administration, R.N.; funding acquisition, R.N. All authors have read and agreed to the published version of the manuscript.

Funding: This research was funded by the Deutsche Forschungsgemeinschaft (DFG), grant number NI489/16-1.

Institutional Review Board Statement: Not applicable.

Informed Consent Statement: Not applicable.

Data Availability Statement: Supplementary crystallographic data can be obtained online free of charge via http://www.ccdc.cam.ac.uk/conts/retrieving.html (accessed on 17 December 2021), deposition numbers CSD 2129567 (Rb_2KAlF_6), 2129568 (K_2AlF_5-2), and 2129569 (K_2AlF_5-3).

Acknowledgments: We thank Sebastian Kunkel for performing the Raman measurements and Falk Lissner for the collection of X-ray intensity data.

Conflicts of Interest: The authors declare no conflict of interest.

References

1. Richter, T.M.M.; Niewa, R. Chemistry of Ammonothermal Synthesis. *Inorganics* **2014**, *2*, 29–78. [CrossRef]
2. Meissner, E.; Niewa, R. *Ammonothermal Synthesis and Crystal Growth of Nitrides: Chemistry and Technology*; Meissner, E., Niewa, R., Eds.; Springer: Cham, Switzerland, 2021; ISBN 9783030563042.
3. Peters, D. Ammonothermal synthesis of aluminum nitride. *J. Cryst. Growth* **1990**, *104*, 411–418. [CrossRef]
4. Purdy, A.P. Ammonothermal Synthesis of Cubic Gallium Nitride. *Chem. Mater.* **1999**, *11*, 1648–1651. [CrossRef]
5. Dwiliński, R.; Baranowski, J.M.; Kamińska, M.; Doradziński, R.; Garczyński, J.; Sierzputowski, L. On GaN Crystallization by Ammonothermal Method. *Acta Phys. Pol. A* **1996**, *90*, 763–766. [CrossRef]
6. Hertrampf, J.; Becker, P.; Widenmeyer, M.; Weidenkaff, A.; Schlücker, E.; Niewa, R. Ammonothermal Crystal Growth of Indium Nitride. *Cryst. Growth Des.* **2018**, *18*, 2365–2369. [CrossRef]
7. Häusler, J.; Schnick, W. Ammonothermal Synthesis of Nitrides: Recent Developments and Future Perspectives. *Chem. Eur. J.* **2018**, *24*, 11864–11879. [CrossRef]
8. Bäucker, C.; Niewa, R. A New Modification of $Rb[Al(NH_2)_4]$ and Condensation in Solid State. *Crystals* **2020**, *10*, 1018. [CrossRef]
9. Bäucker, C.; Bauch, S.; Niewa, R. Synthesis and Characterization of the Amidomanganates $Rb_2[Mn(NH_2)_4]$ and $Cs_2[Mn(NH_2)_4]$. *Crystals* **2021**, *11*, 676. [CrossRef]
10. Becker, P.; Cekovski, T.B.; Niewa, R. Indium Ammoniates from Ammonothermal Synthesis: $InAlF_6(NH_3)_2$, $[In(NH_3)_6][AlF_6]$, and $[In_2F(NH_3)_{10}]_2[SiF_6]_5 \cdot 2\ NH_3$. *Crystals* **2021**, *11*, 679. [CrossRef]
11. Hertrampf, J.; Alt, N.S.A.; Schlücker, E.; Niewa, R. Three Solid Modifications of $Ba[Ga(NH_2)_4]_2$: A Soluble Intermediate in Ammonothermal GaN Crystal Growth. *Eur. J. Inorg. Chem.* **2017**, *2017*, 902–909. [CrossRef]
12. Xiang, H.W. Vapor Pressures, Critical Parameters, Boiling Points, and Triple Points of Ammonia and Trideuteroammonia. *J. Phys. Chem. Ref. Data* **2004**, *33*, 1005–1011. [CrossRef]

13. de Kozak, A.; Gredin, P.; Pierrard, A.; Renaudin, J. The crystal structure of a new form of the dipotassium pentafluoroaluminate hydrate, $K_2AlF_5 \cdot H_2O$, and of its dehydrate, K_2AlF_5. *J. Fluorine Chem.* **1996**, *77*, 39–44. [CrossRef]
14. Schneider, S.; Hoppe, R. Über neue Verbindungen Cs_2NaMF_6 und K_2NaMF_6 sowie über Cs_2KMnF_6. *Z. Anorg. Allg. Chem.* **1970**, *376*, 268–276. [CrossRef]
15. Moras, L.R. Crystal structure of dipotassium sodium fluoroaluminate (elpasolite). *J. Inorg. Nucl. Chem.* **1974**, *36*, 3876–3878. [CrossRef]
16. Graulich, J.; Drüeke, S.; Babel, D. Röntgenstrukturuntersuchungen an den polymorphen Elpasolithen K_2LiAlF_6 und Rb_2LiGaF_6. *Z. Anorg. Allg. Chem.* **1998**, *624*, 1460–1464. [CrossRef]
17. Yakubovich, O.V.; Kiryukhina, G.V.; Dimitrova, O.V. Crystal structure of Rb-elpasolite Rb_2NaAlF_6. *Crystallogr. Rep.* **2013**, *58*, 412–415. [CrossRef]
18. Zhang, S. Intermediates during the Formation of GaN under Ammonothermal Conditions. Ph.D. Thesis, University of Stuttgart, Stuttgart, Germany, 2014.
19. Ehrentraut, D.; Meissner, E.; Bockowski, M. *Technology of Gallium Nitride Crystal Growth*; Ehrentraut, D., Bockowski, M., Meissner, E., Eds.; Springer: Berlin, Germany, 2010; ISBN 9783642048302.
20. Vlasse, M.; Matejka, G.; Tressaud, A.; Wanklyn, B.M. The crystal structure of K_2FeF_5. *Acta Crystallogr. B* **1977**, *33*, 3377–3380. [CrossRef]
21. Le Bail, A.; Desert, A.; Fourquet, J.L. Reinvestigation of the structure of K_2FeF_5. *J. Solid State Chem.* **1990**, *84*, 408–412. [CrossRef]
22. Ma, N.; You, J.; Lu, L.; Wang, J.; Wang, M.; Wan, S. Micro-structure studies of the molten binary K_3AlF_6–Al_2O_3 system by in situ high temperature Raman spectroscopy and theoretical simulation. *Inorg. Chem. Front.* **2018**, *5*, 1861–1868. [CrossRef]
23. Parker, S.F.; Ramirez-Cuesta, A.J.; Daemen, L.L. The structure and vibrational spectroscopy of cryolite, Na_3AlF_6. *RSC Adv.* **2020**, *10*, 25856–25863. [CrossRef]
24. Gilbert, B.; Materne, T. Reinvestigation of Molten Fluoroaluminate Raman Spectra: The Question of the Existence of AlF_5^{2-} Ions. *Appl. Spectrosc. AS* **1990**, *44*, 299–305. [CrossRef]
25. Daniel, P.; Bulou, A.; Rousseau, M.; Nouet, J.; Fourquet, J.L.; Leblanc, M.; Burriel, R. A study of the structural phase transitions in AlF_3: X-ray powder diffraction, differential scanning calorimetry (DSC) and Raman scattering investigations of the lattice dynamics and phonon spectrum. *J. Phys. Condens. Matter* **1990**, *2*, 5663–5677. [CrossRef]
26. Becker, P.; Cekovski, T.B.; Niewa, R. Two Intermediates in Ammonothermal InN Crystal Growth: $[In(NH_3)_5Cl]Cl_2$ and $InF_2(NH_2)$. *Z. Anorg. Allg. Chem.* **2021**, in press. [CrossRef]
27. Alt, N.S.A.; Meissner, E.; Schluecker, E. Development of a novel in situ monitoring technology for ammonothermal reactors. *J. Cryst. Growth* **2012**, *350*, 2–4. [CrossRef]
28. Hertweck, B.; Schimmel, S.; Steigerwald, T.G.; Alt, N.S.A.; Wellmann, P.J.; Schluecker, E. Ceramic liner technology for ammonoacidic synthesis. *J. Supercrit. Fluids* **2015**, *99*, 76–87. [CrossRef]
29. Hüttig, G.F. Apparat zur gleichzeitigen Druck- und Raummessung von Gasen. (Tensi-Eudiometer.). *Z. Anorg. Allg. Chem.* **1920**, *114*, 161–173. [CrossRef]
30. Schimmel, S.; Tomida, D.; Ishiguro, T.; Honda, Y.; Chichibu, S.; Amano, H. Numerical Simulation of Ammonothermal Crystal Growth of GaN—Current State, Challenges, and Prospects. *Crystals* **2021**, *11*, 356. [CrossRef]
31. Erlekampf, J.; Seebeck, J.; Savva, P.; Meissner, E.; Friedrich, J.; Alt, N.S.A.; Schlücker, E.; Frey, L. Numerical time-dependent 3D simulation of flow pattern and heat distribution in an ammonothermal system with various baffle shapes. *J. Cryst. Growth* **2014**, *403*, 96–104. [CrossRef]
32. Sheldrick, G.M. A short history of SHELX. *Acta Crystallogr. A* **2008**, *64*, 112–122. [CrossRef] [PubMed]
33. Sheldrick, G.M. Crystal structure refinement with SHELXL. *Acta Crystallogr. C* **2015**, *71*, 3–8. [CrossRef]